

# Influence of the Solvent Representation on Vibrational Entropy Calculations: Generalized Born Versus Distance-Dependent Dielectric Model

Hannes Kopitz,<sup>[a]</sup> Daniel A. Cashman,<sup>[a]</sup> Stefania Pfeiffer-Marek,<sup>[b]</sup> and Holger Gohlke<sup>\*[a]</sup>

The harmonic model is the most popular approximation for estimating the 'configurational' entropy of a solute in molecular mechanics/Poisson-Boltzmann solvent accessible surface area (MM/PBSA)-type binding free energy calculations. Here, we investigate the influence of the solvent representation in the harmonic model by comparing estimates of changes in the vibrational entropies for 30 trypsin/ligand complexes on ligand binding. Second derivatives of Amber generalized Born (GB) solvation models are available in the nucleic acid builder code. They allow one to use these models for the calculation of vibrational entropies instead of using a simpler solvation model based on a distance-dependent dielectric (DDD) constant. Estimates of changes in the vibrational entropies obtained with a DDD model are systematically and significantly larger, by on average, 6 kcal mol<sup>-1</sup> (at  $T = 300$  K), than estimates obtained with a GB model and so are more favorable for complex formation. The difference becomes larger the more the vibrational entropy contribution disfavors complex formation, that is, the larger the

ligand is (for the complexes considered here). A structural decomposition of the estimates into per-residue contributions reveals polar interactions between the ligand and the surrounding protein, in particular involving charged nitrogens, as a main source of the differences. Snapshots minimized with the DDD model showed a structural deviation from snapshots minimized in explicit water that is larger by, on average, 0.5 Å RMSD compared to snapshots that were minimized with GB<sup>HCT</sup>. As experimental vibrational entropies of biomacromolecules are elusive, there is no direct way to establish a solvent model's superiority. Thus, we can only recommend using the GB harmonic model for vibrational entropy calculations based on the reasoning that smaller structural deviations should point to the implicit solvent model that closer approximates the energy landscape of the solute in explicit solvent. © 2012 Wiley Periodicals, Inc.

DOI: 10.1002/jcc.22933

## Introduction

Perhaps the most troublesome component of computing binding affinities is the estimate of entropic contributions due to changes in the degrees of freedom of the solutes. In molecular mechanics/Poisson-Boltzmann solvent accessible surface area (MM/PBSA)-type calculations of free energies,<sup>1–3</sup> these contributions are estimated in the rigid-rotor, harmonic oscillator approximation. Within this approximation, estimates of changes in the vibrational entropy ( $\Delta S_{\text{vib}}$ ) on complex formation are based on normal mode analysis (NMA),<sup>4,5</sup> owing to the fact that normal mode motions are independent of each other such that the total entropy of a system can be computed by adding the entropy contributions from each mode.<sup>6</sup> As a disadvantage, NMA approximates the potential energy surface of a molecular system by a harmonic function at some minimum on the surface. As such, NMA is unable to consider effects due to population of more than one local minimum, although approaches have been described to overcome this problem.<sup>7</sup>

In practice, for MM/PBSA-type calculations snapshots are extracted from explicit solvent molecular dynamics (MD) simulations, solvent molecules and counter ions are removed, and the solute is subjected to NMA after minimization. Commonly, to account for the effects of a solvent environment during the last two steps, a distance-dependent dielectric (DDD) constant  $\epsilon(r) = 4r$  is applied when calculating Coulombic interactions,

with  $r$  being the distance between two solute atoms.<sup>3,8–10</sup> Compared to this simple model, implicit solvent models provide a more realistic description of the energetic effects of a solvent and counterion environment, while still allowing the solute to be manipulated as though it were an isolated system in gas phase. In that respect, the analytical generalized Born (GB) method provides an approximation to the computationally more intensive Poisson-Boltzmann approach.<sup>11</sup> Recently, second derivatives with respect to Cartesian coordinates have been implemented into the nucleic acid builder (NAB) code for the GB model,<sup>12</sup> as proposed by Still et al.<sup>13</sup> and using the pairwise approach for computing effective Born radii (GB<sup>HCT</sup>) by Hawkins et al.<sup>14</sup> Accordingly, NMA, and hence vibrational entropy calculations, can now be performed within the framework of this continuum solvent model, as demonstrated in a

[a] H. Kopitz, D. A. Cashman, H. Gohlke  
Institute for Pharmaceutical and Medicinal Chemistry, Department of  
Mathematics and Natural Sciences, Heinrich-Heine-University, Düsseldorf,  
Germany  
E-mail: gohlke@uni-duesseldorf.de  
Fax: (+49) 211 81 13847

[b] S. Pfeiffer-Marek  
LGCR Drug Design, Sanofi-Aventis Deutschland GmbH, Frankfurt am Main,  
Germany

Contract/grant sponsor: Sanofi-Aventis Deutschland GmbH.

© 2012 Wiley Periodicals, Inc.

proof-of-principle application<sup>12</sup> for the protein–protein complex formation of Ras-Raf.<sup>3,15</sup> Notably, differences in  $TS_{\text{vib}}$  (at  $T = 300$  K) of up to  $32 \text{ kcal mol}^{-1}$  were found for the proteins in this study, with significantly smaller vibrational entropies obtained when using the  $GB^{\text{HCT}}$  model ( $\Delta S_{\text{vib}}^{\text{GB}}$ ) than when using the DDD model ( $\Delta S_{\text{vib}}^{\text{DDD}}$ ). However, no attempt was made to identify the origin of this discrepancy.<sup>12</sup> Likewise, the use of only one protein–protein complex precluded any conclusion as to whether differences in  $TS_{\text{vib}}$  computed with the  $GB^{\text{HCT}}$  model in general provide a greater stabilization to complex formation than those computed with the DDD model, as observed for the Ras-Raf case.<sup>12</sup>

To investigate the origin of differences between vibrational entropies computed either with  $GB^{\text{HCT}}$  or DDD model in a more systematic fashion, we perform vibrational entropy calculations on a dataset of 30 trypsin/ligand complexes including four peptide ligands and 26 small-molecule ligands. Initially, we investigate the sensitivity of the computed vibrational entropies with respect to the accuracy to which a solute structure has been minimized and with respect to the prefactor in the DDD model. Next, in an endeavor to identify the origin of differences between  $\Delta S_{\text{vib}}^{\text{GB}}$  and  $\Delta S_{\text{vib}}^{\text{DDD}}$  from a structural point of view, we decompose the total vibrational entropy of a system into contributions from single residues, applying a method recently described by Zoete and Michielin.<sup>16</sup> Having identified polar interactions involving nitrogens as sources of the largest differences, we then investigate the influence of different intrinsic GB radii for hydrogens connected to nitrogens, similar to a study of Simmerling and coworkers.<sup>17</sup> Finally, we investigate to what extent structural deviations between snapshots obtained after minimization in explicit solvent or using either the  $GB^{\text{HCT}}$  or the DDD model give rise to the observed  $\Delta S_{\text{vib}}$  differences.

## Materials and Methods

### Dataset of trypsin–ligand complexes

Structures of 30 trypsin/ligand complexes determined by X-ray crystallography to a resolution  $\leq 2.0 \text{ \AA}$  were selected from the Protein Data Bank<sup>18</sup> (PDB codes: 1AYQ, 1C5S, 1F0T, 1G36, 1GJ6, 1K1N, 1K1O, 1K1P, 1MTW, 1O2K, 1O36, 1OX1, 1OYQ, 1QB6, 1QBO, 1QCP, 1RXP, 1S0R, 1SFI, 1TX7, 1V2N, 1Y3W, 2AYW, 2FX4, 2G81, 2PLX, 2ZDK, 2ZDL, 2ZDN, 2ZFS) such that the structures cover a broad spectrum of ligands with varying size, ranging from small ligands like benzamidine, which fills only the S1 pocket of trypsin, to 83mer peptide ligands that form multiple polar and hydrophobic interactions within the trypsin binding pocket. Protonation states of the ligands were determined by the PRODRG webserver (<http://davapc1.bioch.dundee.ac.uk/prodrg/>).<sup>19</sup> Protonation states of histidines and orientations of glutamine and asparagine sidechains were determined by the REDUCE software<sup>20</sup> and were validated by visually inspecting the hydrogen bond network in which each of the residues is involved.

### Molecular dynamics simulations

MD simulations were performed with the AMBER10 package of molecular simulation programs,<sup>21</sup> using the parm99 force field<sup>22</sup> with the “Stony Brook” modification<sup>23</sup> for the receptor and the peptide ligands as well as the gaff force field<sup>24</sup> for the

small-molecule ligands. Force field parameters for benzamidine moieties were taken from McDowell et al.<sup>25</sup> Atomic charges of the small-molecule ligands were derived following the Restrained Electrostatic Potential (RESP)<sup>26</sup> methodology, using a HF/6-31G\* level of theory for the calculation of the electrostatic potential. The complex structures were neutralized with counterions ( $\text{Na}^+$ ,  $\text{Cl}^-$ ) and solvated in an octahedral box of TIP3P water<sup>27</sup> such that the distance between the solute and the boundary of the box was at least  $11 \text{ \AA}$  in all cases.

Then, the complexes were minimized over 50 steps of steepest descent followed by 450 steps of conjugate gradient, while holding the solute fixed by harmonic restraints with force constants of  $25 \text{ kcal mol}^{-1} \text{ \AA}^{-2}$  and  $5 \text{ kcal mol}^{-1} \text{ \AA}^{-2}$ , respectively. Subsequently, the structures were heated from 100 to 300 K, carrying out MD simulations in a canonical ensemble (NVT) for 50 ps, where harmonic restraints with a force constant of  $5 \text{ kcal mol}^{-1} \text{ \AA}^{-2}$  were applied to the solute. Then, the density of the simulation box was adjusted using isothermal-isobaric (NPT) ensemble MD simulations for 50 ps, while still applying harmonic restraints to the solute. Finally, the harmonic restraints were gradually reduced to zero using canonical ensemble MD simulations for an additional 50 ps. The equilibration phase was completed by another 100 ps of canonical ensemble MD simulations without any restraints.

All MD simulations were performed under periodic boundary conditions, treating long-range interactions with the particle mesh Ewald (PME) method<sup>28</sup> with an  $8 \text{ \AA}$ -direct space cut-off and a fourth-order B-spline interpolation. The simulations were run with time steps of 2 fs by freezing bond lengths involving bonds to hydrogen atoms with the SHAKE algorithm.<sup>29</sup> To simulate at a constant temperature of 300 K, the simulation boxes were coupled to an external heat bath using the method of Berendsen et al.<sup>30</sup> with a time constant of 2 ps. Each simulation was carried out for 10 ns. Only the last 6 ns of these production runs were used for the subsequent analyses, and snapshots were extracted at time intervals of 200 ps, resulting in 30 snapshots for each complex structure.

Ten nanosecond of production MD simulation required  $\sim 20$  h on four Intel Core2 Quad CPU Q6600 (16 cores) for one of the smaller complexes (1S0R with 23,324 atoms including solvent) and  $\sim 38$  h for one of the larger complexes (2g81 with 41,197 atoms including solvent).

### Vibrational entropy calculations

NMA for vibrational entropy calculations must proceed from accurate local minima on the energy surface. Here, complex structures from MD simulations were minimized first. Then, starting structures for the separate minimizations of receptor and ligand were taken from these minimized complex structures. This follows a recommendation by Page and Bates<sup>31</sup> according to which, for single trajectory calculations, smaller fluctuations in the computed vibrational entropies are obtained compared to the common approach of extracting starting structures for receptor and ligand from a nonminimized complex structure. For the NMA calculations, all water molecules and counter ions were removed, whereas the structural  $\text{Ca}^{2+}$  ion was retained within the trypsin structure. All atoms of the molecular systems were considered in the NMA calculations, in contrast to truncating the protein structure outside  $\sim 8 \text{ \AA}$  from the ligand as frequently applied. Although the truncation considerably reduces the computational

burden, it can give rise to extensive changes in the molecular geometry on minimization and, subsequently, to large fluctuations in the computed vibrational entropies.<sup>32</sup>

To investigate the influence of how accurately a local minimum on the energy surface is approached on the outcome of a vibrational entropy calculation, we performed NMA on structures minimized to a root-mean-square gradient (RMSG) of the energy of  $<10^{-3}$  kcal mol<sup>-1</sup> Å<sup>-1</sup>,  $<10^{-4}$  kcal mol<sup>-1</sup> Å<sup>-1</sup>, and  $<10^{-10}$  kcal mol<sup>-1</sup> Å<sup>-1</sup>. For the minimizations and NMA calculations, the GB<sup>HCT</sup> model as proposed by Still et al.<sup>13</sup> and using Hawkins et al.<sup>14</sup> pairwise descreening approximation for computing effective Born radii together with *mbondi* intrinsic GB radii was applied. For this, the variables *diel*, *gb*, and *dielc* were set to "C," 1, and 1 in NAB, respectively. As the  $\Delta S_{\text{vib}}$  differences amount to 0.52 cal mol<sup>-1</sup> K<sup>-1</sup> on average when  $S_{\text{vib}}$  is computed from structures minimized to a RMSG  $<10^{-4}$  kcal mol<sup>-1</sup> Å<sup>-1</sup> compared to results computed from structures minimized to a RMSG  $<10^{-10}$  kcal mol<sup>-1</sup> Å<sup>-1</sup> (see Results and Discussion section), all subsequent NMA calculations were based on structures minimized to an RMSG  $<10^{-4}$  kcal mol<sup>-1</sup> Å<sup>-1</sup> for the sake of computational efficiency.

Subsequently, we performed  $S_{\text{vib}}$  calculations using the conventional DDD model. To investigate the influence of the prefactor of the DDD constant, we performed calculations with  $\varepsilon(r) = 1r$ ,  $4r$ , and  $16r$ . For this, the variables *diel*, *gb*, and *dielc* were set to "R94," 0, and {1, 4, 16} in NAB, respectively. As the DDD model has been criticized because of its side-effects due to distorting Coulombic interactions in the protein, we also performed  $S_{\text{vib}}$  calculations using a constant dielectric  $\varepsilon = 1$ .

Finally, we also estimated  $S_{\text{vib}}$  by a quasi-harmonic analysis (QHA) as described in Ref. 3. Here, effective modes are computed such that the second moments of the amplitude distribution match those found in the (explicit solvent) MD simulation. That way, the need to choose a solvation model is avoided, and some of the effects of anharmonic terms in the force field are included in the analysis. To assess the convergence behavior of the QHA results, the production MD simulations of two of the complexes (1QBO, 1S0R) as well as of the unbound receptor and the corresponding ligands were extended to 120 ns. However, even then no converged  $\Delta S_{\text{vib}}$  results were obtained. See Supporting Information for further details on the QHA.

### Structural decomposition of the vibrational entropy

$\Delta S_{\text{vib}}$  estimates obtained by either using GB<sup>HCT</sup> or DDD model significantly differ from each other (see Results and Discussion section). To determine whether these differences have their origin in particular regions within the molecular structures, we repeated the NMA calculations using either solvent model, now performing a per-residue structural decomposition of the vibrational entropy as introduced by Zoete and Michielin.<sup>16</sup> Here, the entropic contribution of a given normal mode is decomposed by attributing to an atom a portion of the entropy proportional to the atom's part in the total vibrational amplitude of this normal mode. By summing atomic contributions over all normal modes, a per-atom contribution to  $S_{\text{vib}}$  is obtained; summing all per-atom contributions of a single residue finally yields a per-residue contribution. It should be noted, however, that while the total entropy is a state function<sup>6</sup> (and, as such, is independent of the pathway used to calculate it), entropy components, in general, are not. Hence, the values of these contributions are sensitive to the decomposition scheme chosen. Still,

the decomposition scheme by Zoete and Michielin<sup>16</sup> has been shown to successfully reproduce entropy differences determined by NMA calculations for which atomic masses of single residues have or have not been set to vanishing values.<sup>15,33</sup> For the DDD model, only  $\varepsilon(r) = 4r$  was used here.

### Altering intrinsic GB radii of nitrogen-bound hydrogens

The structural decomposition of vibrational entropies revealed polar interactions involving nitrogens as sources of the largest differences between  $\Delta S_{\text{vib}}^{\text{GB}}$  and  $\Delta S_{\text{vib}}^{\text{DDD}}$  (see Results and Discussion section). Previously, salt bridges involving charged nitrogens have been observed to be frequently too stable in the GB implicit solvent model,<sup>34–36</sup> and this effect has been counterbalanced by modifying the intrinsic radii of hydrogen atoms of charged protein groups.<sup>17</sup> To investigate the influence such modified intrinsic GB radii may have on computed  $\Delta S_{\text{vib}}^{\text{GB}}$  values, we tested the following dielectric radii sets, in addition to the *mbondi* set: (1) we reduced the radii of hydrogens connected to charged nitrogens in Arg, Lys, and N-terminal ammonium groups (parm99 atom types N2 and N3<sup>37</sup>) as well as all charged nitrogens in the ligands from 1.3 to 1.1 Å. This radii set is referred to as *mbondi-s* below. (2) We used the *mbondi* radii set as implemented in AMBER6, which is referred to as *amber6* in the AMBER10 version. Here, the radius of a hydrogen atom connected to a nitrogen is 1.2 Å, irrespective of the nitrogen atom type. (3) We combined sets (1) and (2) by setting the radii of hydrogens connected to charged nitrogens to 1.1 Å, and to 1.2 Å for hydrogens connected to any other nitrogen. We refer to this set as *amber6-s* below.

### Explicit solvent minimizations

The minimization of the complex structures in explicit solvent (TIP3P) was done with the SANDER module of AMBER10 using periodic boundary conditions to treat long range interactions with PME and applying the conjugate gradient method until the RMSG reached  $<10^{-2}$  kcal mol<sup>-1</sup> Å<sup>-1</sup>. To compare these minimized structures to structures minimized in implicit solvent, all solvent molecules were removed, and the RMSD of all atoms was calculated with the PTRAJ module of AMBER10.

## Results and Discussion

### Accuracy of minimization has little impact on the computed vibrational entropy differences

For the description of the dynamics of a system in terms of normal mode directions and frequencies, the system must reside at a local minimum on the potential energy surface where the energy gradient vanishes.<sup>38</sup> Hence, distorted molecular structures, such as snapshots extracted from MD trajectories, must be minimized before performing NMA. In MM/PBSA-type of applications, typically, structures have been minimized to a root-mean-square gradient of the potential energy of  $10^{-5}$ – $10^{-3}$  kcal mol<sup>-1</sup> Å<sup>-1</sup> before calculating vibrational entropies via NMA.<sup>3</sup> In other applications, highly accurate minima with RMSG  $<10^{-12}$  kcal mol<sup>-1</sup> Å<sup>-1</sup> have been described to be required to prevent low-frequency normal modes to be contaminated with overall translational and rotational character.<sup>12</sup> Thus, from an application point of view, it is of interest to determine the influence of

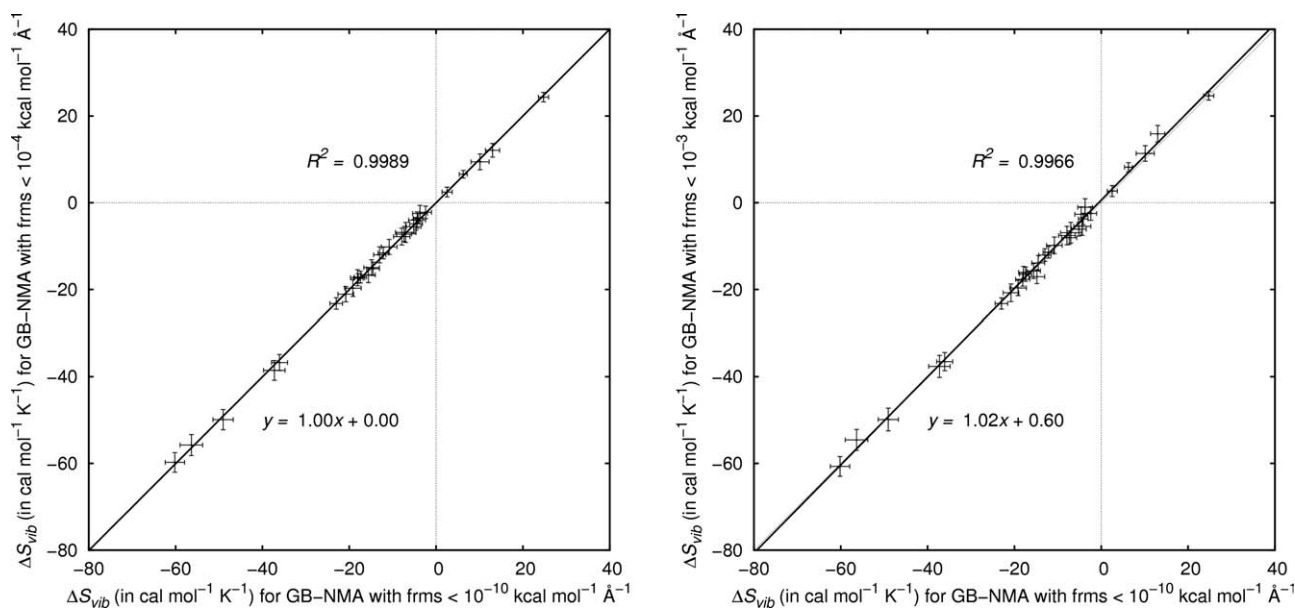


**Figure 1.** Influence of the accuracy of minimization on computed vibrational entropy differences.  $\Delta S_{\text{vib}}$  computed on structures minimized to a)  $\text{RMSG} < 10^{-4} \text{ kcal mol}^{-1} \text{ \AA}^{-1}$  and b)  $\text{RMSG} < 10^{-3} \text{ kcal mol}^{-1} \text{ \AA}^{-1}$  are plotted versus  $\Delta S_{\text{vib}}$  computed on structures minimized to  $\text{RMSG} < 10^{-10} \text{ kcal mol}^{-1} \text{ \AA}^{-1}$ . Both types of calculations were performed with the  $\text{GB}^{\text{HCT}}$  model.

the accuracy of minimization on the outcome of vibrational entropy calculations, in particular, in view of the fact that computationally demanding Newton–Raphson minimization is required to obtain a  $\text{RMSG}$  as low as  $10^{-12} \text{ kcal mol}^{-1} \text{ \AA}^{-1}$ .

Results for vibrational entropy differences calculated as averages of  $\Delta S_{\text{vib}} = S_{\text{vib, complex}} - (S_{\text{vib, trypsin}} + S_{\text{vib, ligand}})$  over 30 snapshots each and based on structures minimized to  $\text{RMSG} < 10^{-3}$ ,  $10^{-4}$ , or  $10^{-10} \text{ kcal mol}^{-1} \text{ \AA}^{-1}$  are given in Figure 1. Results for intermediate  $\text{RMSG}$  between  $10^{-4}$  and  $10^{-10} \text{ kcal mol}^{-1} \text{ \AA}^{-1}$  are not available due to the fact that, in many cases, the Newton–Raphson minimizer required only one iteration to reach a  $\text{RMSG}$  of  $\sim 10^{-10} \text{ kcal mol}^{-1} \text{ \AA}^{-1}$  when starting from structures with a  $\text{RMSG}$  of  $\sim 10^{-4} \text{ kcal mol}^{-1} \text{ \AA}^{-1}$ . A detailed listing of computed  $\Delta S_{\text{vib}}$  is given in Supporting Information, Table S1.

$\Delta S_{\text{vib}}$  results obtained from structures minimized to  $\text{RMSG} < 10^{-4} \text{ kcal mol}^{-1} \text{ \AA}^{-1}$  almost perfectly agree with those obtained from structures minimized to  $\text{RMSG} < 10^{-10} \text{ kcal mol}^{-1} \text{ \AA}^{-1}$ , as demonstrated by a correlation coefficient  $R^2 = 0.9987$  and a mean (maximal) absolute difference of  $0.52 \text{ cal mol}^{-1} \text{ K}^{-1}$  ( $1.28 \text{ cal mol}^{-1} \text{ K}^{-1}$ ; PDB-code 1SFI), which leads to a mean (maximal) absolute difference of the contribution to the binding free energy  $T\Delta S_{\text{vib}}$  at  $T = 300 \text{ K}$  of  $0.16 \text{ kcal mol}^{-1}$  ( $0.38 \text{ kcal mol}^{-1}$ ). On some occasions, large standard deviations of computed  $\Delta S_{\text{vib}}$  values have been reported, owing to deviating molecular geometries subjected to NMA.<sup>32</sup> Here, no influence of the  $\text{RMSG}$  criterion on the standard deviation is found, as demonstrated by standard errors (calculated as standard deviation/ $\sqrt{N}$  with  $N = 30$ ) of  $1.69 \text{ cal mol}^{-1} \text{ K}^{-1}$  for both, the  $10^{-10} \text{ kcal mol}^{-1} \text{ \AA}^{-1}$  and  $10^{-4} \text{ kcal mol}^{-1} \text{ \AA}^{-1}$ -based calculations. Using a less strict  $\text{RMSG}$  criterion of  $< 10^{-3} \text{ kcal mol}^{-1} \text{ \AA}^{-1}$  does not deteriorate the agreement of  $\Delta S_{\text{vib}}$  results with those obtained for  $10^{-10} \text{ kcal mol}^{-1} \text{ \AA}^{-1}$ -based structures, as shown by a correlation

coefficient  $R^2 = 0.9962$  and a mean (maximal) absolute difference of  $0.91 \text{ cal mol}^{-1} \text{ K}^{-1}$  ( $2.91 \text{ cal mol}^{-1} \text{ K}^{-1}$ ; PDB-code 2FX4).

Although accuracy and precision of  $\Delta S_{\text{vib}}$  remain essentially unchanged, the computational burden is rather different when computing vibrational entropies based on structures minimized to either  $\text{RMSG} < 10^{-4} \text{ kcal mol}^{-1} \text{ \AA}^{-1}$  ( $10^{-3} \text{ kcal mol}^{-1} \text{ \AA}^{-1}$ ) or  $\text{RMSG} < 10^{-10} \text{ kcal mol}^{-1} \text{ \AA}^{-1}$ . The overall process of computing  $\Delta S_{\text{vib}}$  in the former case requires, on average, only 55% (43%) of the computational time required for the latter case. As such, on a per snapshot basis, the minimization of a small complex (1S0R) to  $\text{RMSG} < 10^{-10} \text{ kcal mol}^{-1} \text{ \AA}^{-1}$  required  $\sim 9.5 \text{ h}$  and the subsequent NMA  $\sim 2.75 \text{ h}$  on one core of an Intel Core2 Quad CPU Q6600, whereas a minimization to  $\text{RMSG} < 10^{-4} \text{ kcal mol}^{-1} \text{ \AA}^{-1}$  required only  $\sim 4.5 \text{ h}$ . For the largest complex (2G81),  $\sim 14 \text{ h}$  were required for a minimization to  $\text{RMSG} < 10^{-10} \text{ kcal mol}^{-1} \text{ \AA}^{-1}$  and  $\sim 2.85 \text{ h}$  for the subsequent NMA, whereas a minimization to  $\text{RMSG} < 10^{-4} \text{ kcal mol}^{-1} \text{ \AA}^{-1}$  required only  $\sim 9.5 \text{ h}$ . Based on these findings, we decided to perform subsequent NMA calculations using structures minimized to  $\text{RMSG} < 10^{-4} \text{ kcal mol}^{-1} \text{ \AA}^{-1}$ .

#### $\Delta S_{\text{vib}}^{\text{DDD}}$ results systematically deviate from $\Delta S_{\text{vib}}^{\text{GB}}$ results

In contrast to the accuracy of the minimization, the solvent representation has a major impact on computed  $\Delta S_{\text{vib}}$  values (Fig. 2).  $\Delta S_{\text{vib}}$  results obtained using a DDD model with  $\varepsilon(r) = 4r$  are systematically larger than  $\Delta S_{\text{vib}}$  values obtained by using the  $\text{GB}^{\text{HCT}}$  model, resulting in a mean (maximal) absolute difference of  $20.19 \text{ cal mol}^{-1} \text{ K}^{-1}$  ( $46.58 \text{ cal mol}^{-1} \text{ K}^{-1}$ ; PDB-code 2G81). Using  $\varepsilon(r) = 1r$  or  $16r$  did not qualitatively change this finding. Hence, all subsequent  $\Delta S_{\text{vib}}^{\text{DDD}}$  results are reported for  $\varepsilon(r) = 4r$ . With respect to the contribution to the binding free energy at  $T = 300 \text{ K}$ ,  $T\Delta S_{\text{vib}}^{\text{DDD}}$  is on average (at most), larger by  $6.06 \text{ kcal mol}^{-1}$  ( $13.97$



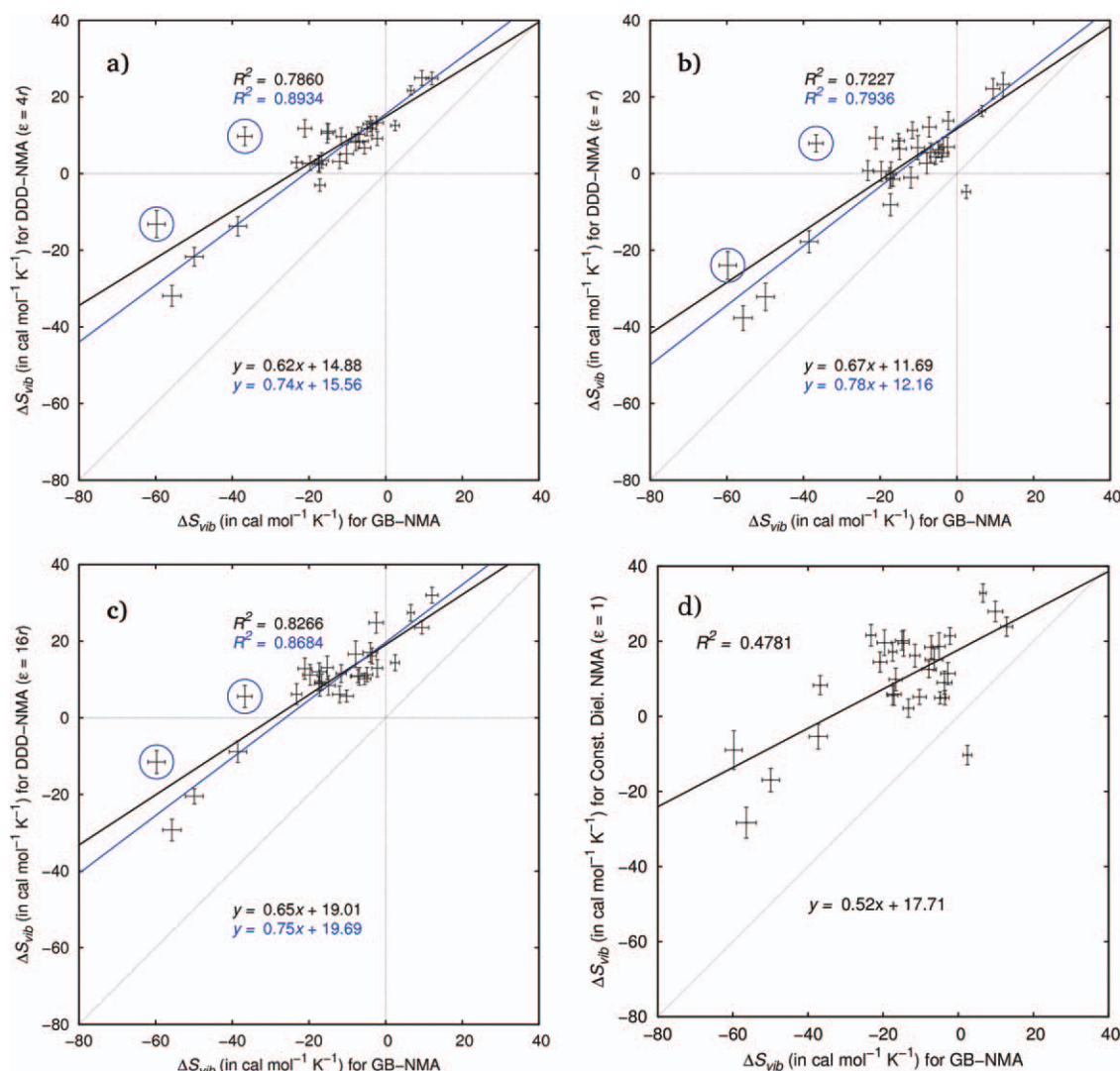


**Figure 2.** Influence of the solvent model on computed vibrational entropy differences.  $\Delta S_{\text{vib}}$  computed using the DDD model with a)  $\varepsilon(r) = 4r$ , b)  $\varepsilon(r) = r$ , and c)  $\varepsilon(r) = 16r$  as well as applying a constant dielectric of d)  $\varepsilon = 1$  are plotted versus  $\Delta S_{\text{vib}}$  computed using the GB<sup>HCT</sup> model. All NMA calculations are based on structures minimized to  $\text{RMSG} < 10^{-4}$  kcal mol<sup>-1</sup> Å<sup>-1</sup>. Error bars show the standard error of the mean. Correlation values are shown when all data points are included (black) as well as when data points for PDB codes 1AQ7 and 2G81 are omitted (blue).

kcal mol<sup>-1</sup>) than  $T\Delta S_{\text{vib}}^{\text{GB}}$ . Thus, contributions due to changes in the vibrational degrees of freedom are more favorable for complex formation if computed with the DDD model. This finding is in agreement with results on the protein–protein complex Ras-Raf in the work of Brown and Case.<sup>12</sup> We note that the differences between  $\Delta S_{\text{vib}}^{\text{DDD}}$  and  $\Delta S_{\text{vib}}^{\text{GB}}$  exceed the standard error in these values by at least a factor of four for all trypsin/ligand complexes and, hence, do have a significant effect on the binding free energy estimates. In fact, for 21 of 30 complexes, these differences lead to  $T\Delta S_{\text{vib}}^{\text{GB}}$  values disfavoring complex formation, whereas the respective  $T\Delta S_{\text{vib}}^{\text{DDD}}$  values favor the bound state. Furthermore, the difference between  $\Delta S_{\text{vib}}^{\text{DDD}}$  and  $\Delta S_{\text{vib}}^{\text{GB}}$  is not constant but becomes larger the more the vibrational entropy contribution disfavors complex formation, as demonstrated by a correlation line with a slope  $< 1$ . In the case of the trypsin ligand complexes, this means that complexes with the largest ligands (in particular, the peptide ligands) show the largest differences between models.

Using a constant dielectric  $\varepsilon = 1$  instead of the DDD model results in larger standard errors of computed  $\Delta S_{\text{vib}}$ , a signifi-

cantly worse correlation with respect to values obtained with the GB<sup>HCT</sup> model, and a more pronounced dependence of the differences of  $\Delta S_{\text{vib}}$  values on the ligand size (Fig. 2d).

### Structural decomposition reveals polar interactions as main sources of differences between $\Delta S_{\text{vib}}^{\text{GB}}$ and $\Delta S_{\text{vib}}^{\text{DDD}}$

Next, we aimed to identify the origin of differences between  $\Delta S_{\text{vib}}^{\text{GB}}$  and  $\Delta S_{\text{vib}}^{\text{DDD}}$  values from a structural point of view. Decomposing the vibrational entropy difference into contributions from residues<sup>16</sup> reveals a complex picture in that respect. First, in all but one (PDB-code 2FX4) case, the ligand contributes most to the difference. Second, with respect to trypsin residues, Asp171 shows the largest contribution in four trypsin–ligand cases, Ser172 in 12 cases, Gln174 in four cases, Ser177 in four cases, Gly196 in four cases, Asn 79 in one case (PDB-code 2PLX), and Gln155 in another case (PDB-code 2G81). All these residues are in the immediate vicinity of the ligand:  $\Delta S_{\text{vib}}$  originates mostly from changes in the vibrational

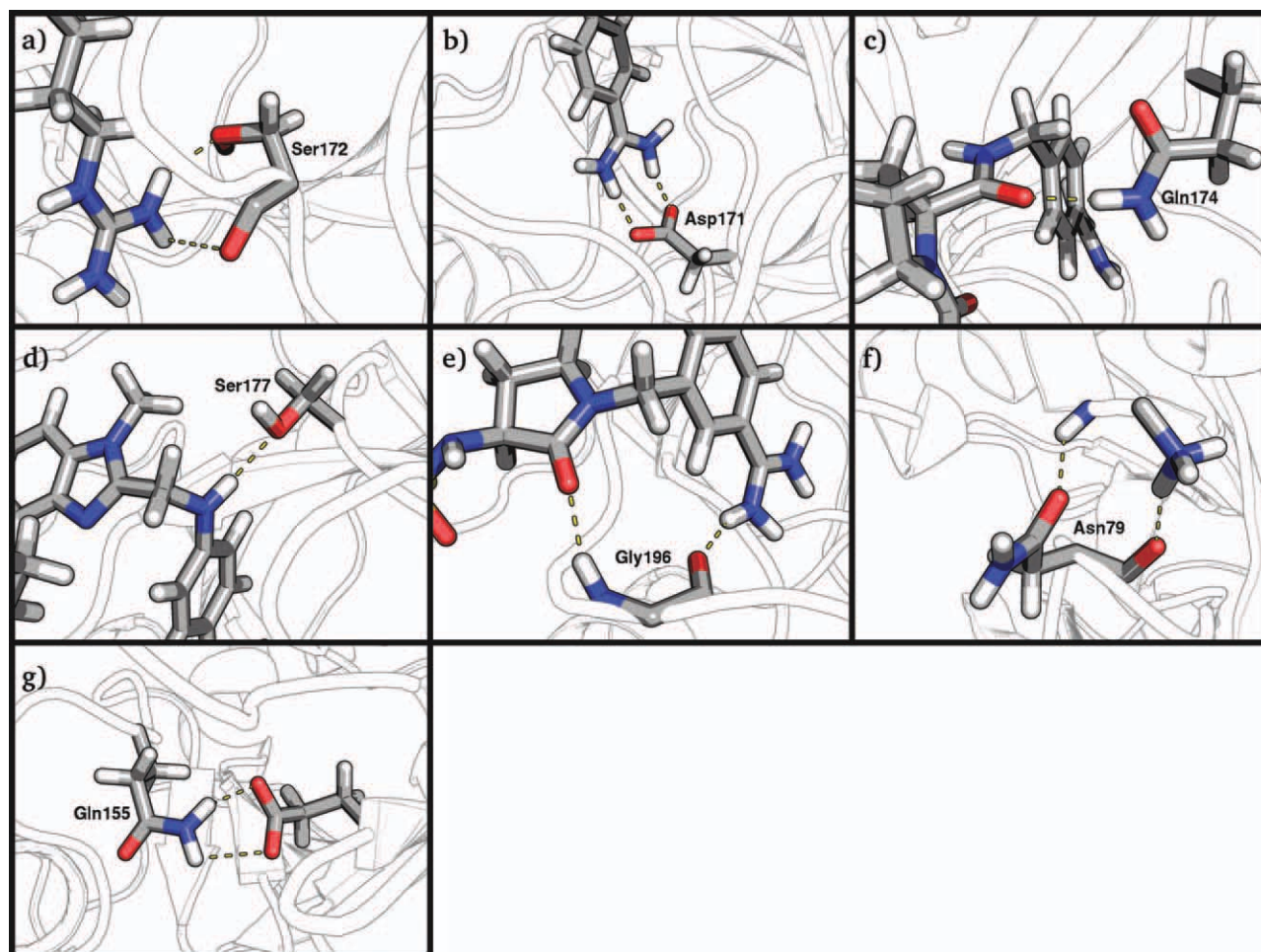


**Figure 3.** Interactions between the ligand and that residue of the receptor that shows the largest difference between  $\Delta S_{\text{vib}}$  computed with either the  $\text{GB}^{\text{HCT}}$  or DDD model in a pair-wise structural decomposition. All snapshots have been minimized using the  $\text{GB}^{\text{HCT}}$  model together with the *mbondi* radii. a) H-bonds between the sidechain hydroxyl group of Ser172 as well as its backbone amide oxygen and the guanidine moiety of the ligand (PDB code: 1AQ7); b) salt-bridge between Asp171 and the benzamidine moiety of the ligand (PDB code: 2AYW); c) H-bond between the sidechain amide nitrogen of Gln174 and an amide oxygen of the ligand (PDB code: 2ZDK); d) H-bond between the hydroxyl group of Ser177 and an amine group of the ligand (PDB code: 1OYQ); e) two H-bonds involving the backbone amide group of Gly196 (PDB code: 1F0T): The first one is formed between the amide nitrogen of Gly196 and an amide oxygen of the ligand, the second one between the amide oxygen of Gly196 and the amidine moiety of the ligand; f) two H-bonds between Asn79 and a peptide ligand (PDB code: 2PLX): The first one is formed between the backbone amide oxygen of Asn79 and the *N*-terminus of the first residue of the ligand, the second one between the sidechain amide oxygen of Asn79 and the backbone amide nitrogen of the second residue of the ligand; g) two H-bonds between the sidechain amide nitrogen of Gln155 of the receptor and the carboxy group of Glu7 of the peptide ligand (PDB code: 2G81).

degrees of freedom of residues to which the ligand forms direct interactions in the complex. Unsurprisingly, the largest differences between contributions to  $\Delta S_{\text{vib}}^{\text{GB}}$  and  $\Delta S_{\text{vib}}^{\text{DDD}}$  are then found for the ligand and neighboring trypsin residues, too.

More fundamentally, all the above trypsin residues interact via hydrogen bonds with the ligand, and many of these hydrogen bonds involve a ligand moiety with a charged nitrogen: (i) the hydroxyl group and the carbonyl oxygen of Ser172 form hydrogen bonds with the amidino/guanidino group of the ligand (Fig. 3a); (ii) the sidechain of Asp171 forms a salt bridge to the amidino/guanidino group of the ligand (Fig. 3b); (iii) Gln174 is involved in a hydrogen bond between the sidechain amide group and a carbonyl oxygen of the ligand (Fig. 3c); (iv) the hydroxyl group (amide nitrogen) of Ser177 interacts with an anilino nitrogen (carbonyl oxygen) of the ligand (Fig. 3d); V), the amide group of Gly196 forms hydrogen bonds with the

amidino/guanidino group of the ligand and with a ligand's carbonyl oxygen (Fig. 3e). Finally, in two complexes with a peptide ligand, the carbonyl oxygen of Asn79 forms a hydrogen bond with the *N*-terminus of the peptide (Fig. 3f), and the sidechain amide group of Gln155 interacts with the sidechain of a peptide's glutamate (Fig. 3g).

#### Modification of intrinsic GB radii of nitrogen-bound hydrogens does not change $\Delta S_{\text{vib}}^{\text{GB}}$ results

The finding that  $\Delta S_{\text{vib}}^{\text{GB}}$  values are consistently smaller than  $\Delta S_{\text{vib}}^{\text{DDD}}$  values suggests a more tightly bound ligand in the case of the  $\text{GB}^{\text{HCT}}$  model. Furthermore, the findings from the structural decomposition suggest that it may be differences between the  $\text{GB}^{\text{HCT}}$  and DDD model in describing interactions with (charged) nitrogens that lead to a more tightly bound ligand.

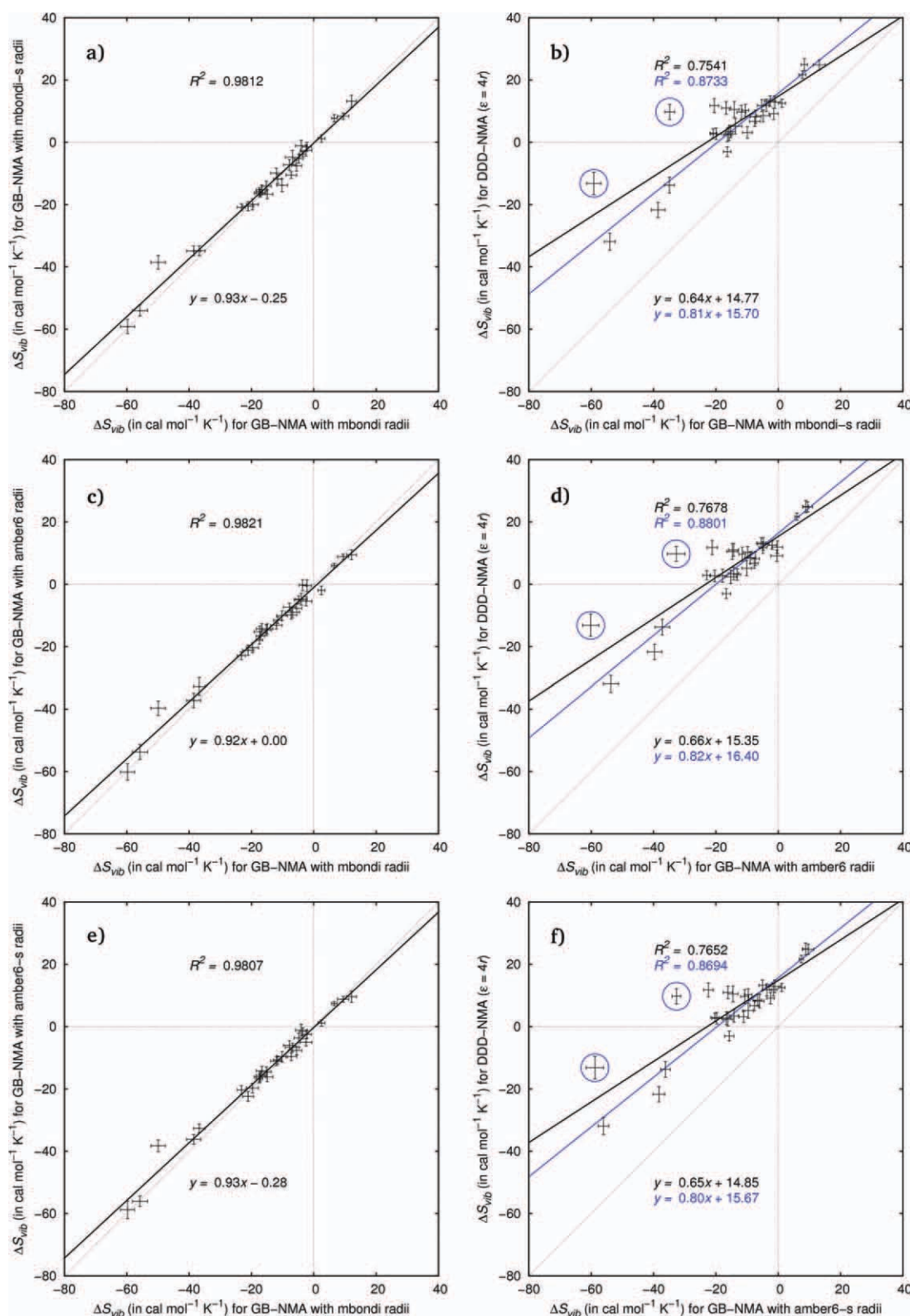


**Figure 4.** Influence of the intrinsic dielectric radii on computed vibrational entropy differences. a)  $\text{GB}^{\text{HCT}}$  model with *mbondi* radii versus  $\text{GB}^{\text{HCT}}$  model with *mbondi-s* radii; b)  $\text{GB}^{\text{HCT}}$  model with *mbondi-s* radii versus DDD model using  $\varepsilon(r) = 4r$ ; c)  $\text{GB}^{\text{HCT}}$  model with *mbondi* radii versus  $\text{GB}^{\text{HCT}}$  model with *amber6* radii; d)  $\text{GB}^{\text{HCT}}$  model with *amber6* radii versus DDD model with  $\varepsilon(r) = 4r$ ; e)  $\text{GB}^{\text{HCT}}$  model with *mbondi* radii versus  $\text{GB}^{\text{HCT}}$  model with *amber6-s* radii; f)  $\text{GB}^{\text{HCT}}$  model with *amber6-s* radii versus DDD model with  $\varepsilon(r) = 4r$ . All NMA calculations are based on structures minimized to  $\text{RMSG} < 10^{-4} \text{ kcal mol}^{-1} \text{ \AA}^{-1}$ . Error bars show the standard error of the mean. Correlation values are shown when all data points are included (black) as well as when data points for PDB codes 1AQ7 and 2G81 are omitted (blue). [Color figure can be viewed in the online issue, which is available at [wileyonlinelibrary.com](http://wileyonlinelibrary.com).]



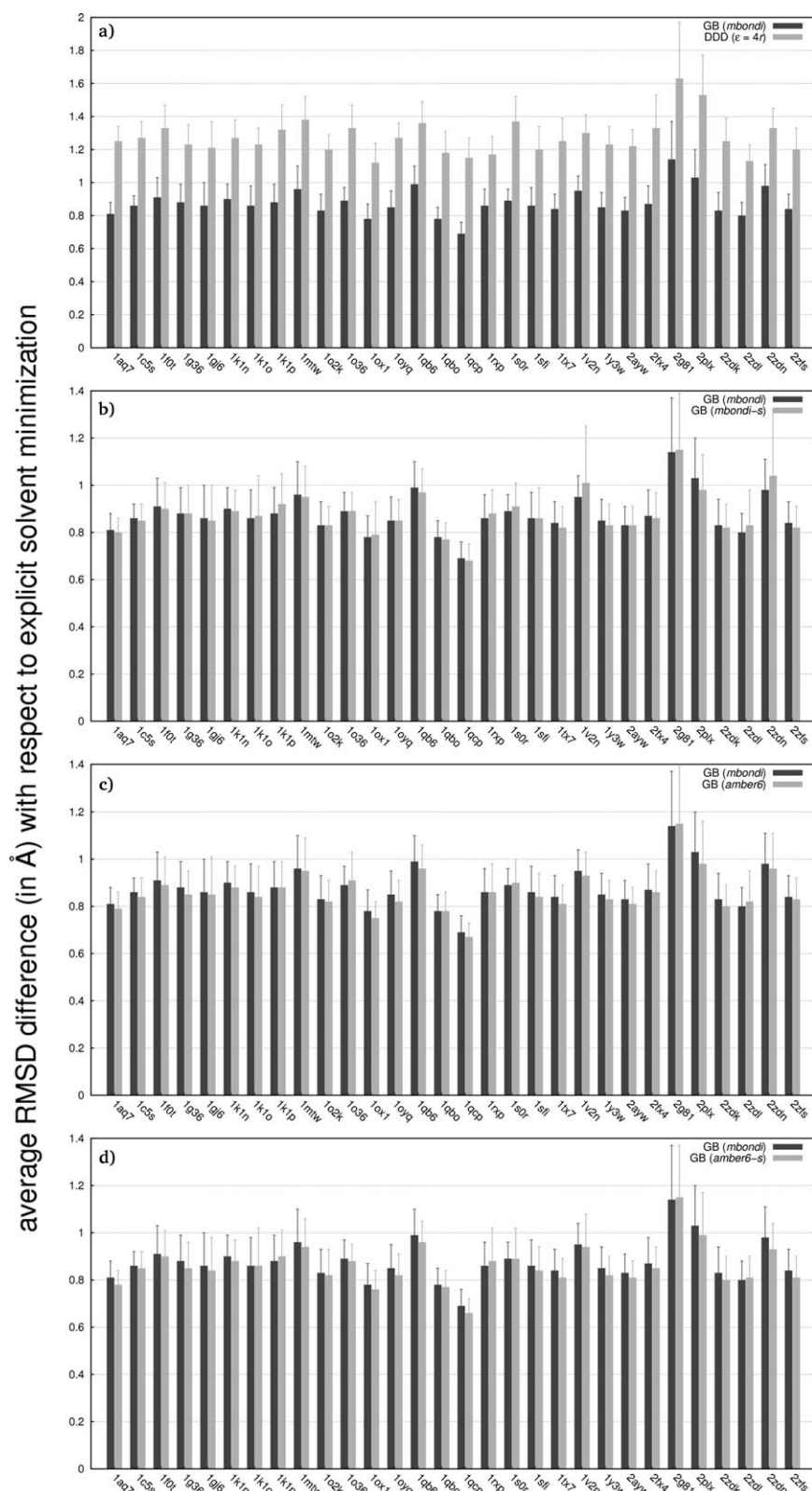


**Figure 5.** Structural deviation of snapshots minimized with an implicit solvent model with respect to snapshots minimized in explicit solvent. a)  $\text{GB}^{\text{HCT}}$  model with *mbondi* radii versus DDD model with  $\varepsilon(r) = 4r$ ; b)  $\text{GB}^{\text{HCT}}$  model with *mbondi* radii versus  $\text{GB}^{\text{HCT}}$  model with *mbondi-s* radii; c)  $\text{GB}^{\text{HCT}}$  model with *mbondi* radii versus  $\text{GB}^{\text{HCT}}$  model with *amber6* radii. d)  $\text{GB}^{\text{HCT}}$  model with *mbondi* radii versus  $\text{GB}^{\text{HCT}}$  model with *amber6-s* radii. Bars denote the RMSD of all atoms averaged over 30 structures for each complex. Error bars show the standard error of the mean.

These suggestion point to recent studies that showed that the applied GB model overstabilizes salt-bridges; this holds particularly for those salt-bridges that involve positively charged nitrogens.<sup>34–36,39,40</sup> Accordingly, we investigated the influence of different intrinsic GB radii for hydrogens connected to nitrogens on the outcome of  $\Delta S_{\text{vib}}^{\text{GB}}$  calculations by repeating all minimizations and NMA calculations with the *mbondi-s*, *amber6*, and *amber6-s* radii sets (see Materials and Methods Section). This approach is similar to a study of Simmerling and coworkers,<sup>17</sup> who obtained significantly improved results for potential of mean force calculations of the formation of salt bridges by reducing such intrinsic GB radii. The rationale for this finding is that the reduced radius of hydrogen connected to nitrogen effectively increases the desolvation penalty of the nitrogen-containing group and, in turn, destabilizes polar or salt-bridge interactions formed with this group.

Results for the modified radii sets are given in Figure 4. In all three cases, changing the intrinsic GB radii only had a marginal effect when compared with the *mbondi* set, as demonstrated by correlation coefficients  $R^2 > 0.98$ . Furthermore, the systematic difference between  $\Delta S_{\text{vib}}^{\text{GB}}$  and  $\Delta S_{\text{vib}}^{\text{DDD}}$  did not decrease either. This insensitivity of  $\Delta S_{\text{vib}}^{\text{GB}}$  results with respect to variations in the intrinsic GB radii was unexpected. Apparently, although the reduced radii do lead to a marked destabilization of the salt-bridge interaction,<sup>17</sup> the accompanying change in the curvature of the potential energy surface at the minimum of this interaction is small (see also Fig. 4 in Ref. 17), resulting in a likewise small change of the  $\Delta S_{\text{vib}}^{\text{GB}}$  estimate.

Are structural deviations of snapshots minimized using either implicit solvent model the cause for differences in  $\Delta S_{\text{vib}}$  estimates?

From the above results, we anticipated that  $\Delta S_{\text{vib}}$  estimates are rather insensitive to the representation of a single interaction. This is confirmed, in a broader sense, by our observation that choosing  $\varepsilon(r) = 1r$  or  $16r$  instead of  $4r$  did not qualitatively change the differences between  $\Delta S_{\text{vib}}^{\text{GB}}$  and  $\Delta S_{\text{vib}}^{\text{DDD}}$  estimates



either. Hence, we concluded that the difference between  $\Delta S_{\text{vib}}^{\text{GB}}$  and  $\Delta S_{\text{vib}}^{\text{DDD}}$  must have its origin in a more global effect due to the  $\text{GB}^{\text{HCT}}$  or DDD model. In the context of using truncated protein structures as input to  $\Delta S_{\text{vib}}$  calculations, a previous study has already pointed to structural deviations of minimized snapshots as a cause for differences in  $\Delta S_{\text{vib}}$  estimates.<sup>32</sup> However, the influence of the solvent representation during the minimization step on the molecular geometries and, hence, the subsequent  $\Delta S_{\text{vib}}$  estimates has not yet been investigated. Thus, we minimized snapshots taken from a thermalized ensemble of a MD simulation in explicit solvent. The resulting molecular geometries were used as starting points for minimizations with either the  $\text{GB}^{\text{HCT}}$  or DDD model. Finally, the root-mean-square deviations (RMSD) with respect to all atoms between the  $\text{GB}^{\text{HCT}}$ -/DDD-minimized and the explicit solvent-minimized structures were determined.

These results are shown in Figure 5. A perfect agreement between protein structures minimized in explicit or implicit solvent cannot be expected. As one reason, the implicit solvent model does not take into account structural water molecules that can have a strong effect on solute structure and energetics.<sup>41</sup> Still, one can assume that smaller deviations between the minimized structures should point to the implicit solvent model that better approximates the energy landscape of the solute in explicit solvent. As expected, the mean RMSD values for trypsin structures minimized with the  $\text{GB}^{\text{HCT}}$  model are 0.8 Å, whereas the RMSD values for structures minimized with the DDD model are larger by, on average, 0.5 Å.

Finally, we intended to investigate to what extent differences in the structural deviations of snapshots give rise to differences in  $\Delta S_{\text{vib}}$ . For this, we took snapshots initially minimized using the DDD model and reminimized them using the  $\text{GB}^{\text{HCT}}$  model (hereafter called 'DDD- $\text{GB}^{\text{HCT}}$  snapshots'), after which we calculated  $\Delta S_{\text{vib}}^{\text{GB}}$ . We expected that this will lead to minimized structures that deviate less from the DDD-minimized ones than if the minimization was started on snapshots from MD simulation and the  $\text{GB}^{\text{HCT}}$  model was used right from the beginning (hereafter called ' $\text{GB}^{\text{HCT}}$  snapshots'). We then wanted to see whether  $\Delta S_{\text{vib}}^{\text{GB}}$  is closer to  $\Delta S_{\text{vib}}^{\text{DDD}}$  for the DDD- $\text{GB}^{\text{HCT}}$  snapshots. Unfortunately, our expectations were not met because DDD- $\text{GB}^{\text{HCT}}$  snapshots did not stay close to the starting structures but ended up being structurally closer to  $\text{GB}^{\text{HCT}}$  snapshots (data not shown). Conversely, snapshots initially minimized using the  $\text{GB}^{\text{HCT}}$  model and reminimized with the DDD model became structurally closer to DDD snapshots (data not shown). Unfortunately, this precludes providing an answer to what extent differences in the structural deviations of snapshots give rise to differences in  $\Delta S_{\text{vib}}$ .

## Conclusions

We have investigated the influence of the solvent representation in the harmonic model on vibrational entropy calculations, using a dataset of 30 trypsin/ligand complexes. Despite its inherent limitations, the harmonic model is the most popular approximation for estimating the 'configurational' entropy of a solute in MM/PBSA-type (binding) free energy calculations. Initial computations revealed that the accuracy of minimization has little

impact on  $\Delta S_{\text{vib}}$  in that  $\Delta S_{\text{vib}}$  obtained from structures minimized to  $\text{RMSG} < 10^{-3} \text{ kcal mol}^{-1} \text{ Å}^{-1}$  almost perfectly agree with those obtained from structures minimized to  $\text{RMSG} < 10^{-10} \text{ kcal mol}^{-1} \text{ Å}^{-1}$ . However, using the less strict RMSG criterion saves, on average, 57% of the computational time required in the latter case. This finding may be worth considering when MM/PBSA-type calculations are applied to larger datasets of receptor-ligand complexes, such as for rescoring docking hit lists.<sup>42</sup>

The most outstanding result here is the extent to which the solvent representation impacts  $\Delta S_{\text{vib}}$  calculations:  $\Delta S_{\text{vib}}$  results obtained with any of the DDD models tested here are systematically and significantly larger than those obtained with the  $\text{GB}^{\text{HCT}}$  model (on average  $6.06 \text{ kcal mol}^{-1}$  at  $T = 300 \text{ K}$ ) and, thus, are more favorable for complex formation. For  $\sim 2/3$  of the trypsin complexes, this leads to opposing contributions of  $T\Delta S_{\text{vib}}$  to the binding free energy, which may have a large influence when it comes to applying MM/PBSA free energies for ranking virtual screening hit lists.<sup>43</sup> Furthermore, the differences between  $\Delta S_{\text{vib}}^{\text{DDD}}$  and  $\Delta S_{\text{vib}}^{\text{GB}}$  become the larger the more the vibrational entropy contribution disfavors complex formation; i.e., the differences increase with increasing size of the ligands (for the complexes considered here).


A structural decomposition revealed polar interactions between the ligand and residues in the immediate vicinity as the main sources of  $\Delta S_{\text{vib}}$  differences; many of these interactions are hydrogen bonds to a ligand moiety with a charged nitrogen. However, attempts to reduce the intrinsic GB radii of nitrogen-attached hydrogens to counteract presumably too strong polar hydrogen bonds or salt bridges did not show any effect. Finally, snapshots minimized with the DDD model showed a structural deviation from snapshots minimized in explicit water that is larger than if the snapshots were minimized with  $\text{GB}^{\text{HCT}}$ . As experimental vibrational entropies of biomacromolecules are elusive, there is no direct way to establish a solvent model's superiority. Thus, we can only recommend using the GB harmonic model for vibrational entropy calculations based on the reasoning that smaller structural deviations should point to the implicit solvent model that closer approximates the energy landscape of the solute in explicit solvent.

## Acknowledgments

The authors are grateful to the Zentrum fuer Informations-und Medientechnologie (ZIM) at the Heinrich-Heine-University, Duesseldorf, for computational support.

**Keywords:** protein–ligand binding • molecular recognition • binding free energy • AMBER • NAB

How to cite this article: H. Kopitz, D. A. Cashman, S. Pfeiffer-Marek, H. Gohlke, *J. Comput. Chem.* **2012**, *00*, 00–00. DOI: 10.1002/jcc.22933

 Additional Supporting Information may be found in the online version of this article.

[1] J. Srinivasan, T. E. Cheatham, III, P. Cieplak, P. A. Kollman, D. A. Case, *J. Am. Chem. Soc.* **1998**, *120*, 9401.

- [2] P. A. Kollman, I. Massova, C. Reyes, B. Kuhn, S. Huo, L. Chong, M. Lee, T. Lee, Y. Duan, W. Wang, O. Donini, P. Cieplak, J. Srinivasan, D. A. Case, T. E. Cheatham, III, *Acc. Chem. Res.* **2000**, *33*, 889.
- [3] H. Gohlke, D. A. Case, *J. Comput. Chem.* **2004**, *25*, 238.
- [4] N. Go, H. A. Scheraga, *J. Chem. Phys.* **1969**, *51*, 4751.
- [5] N. Go, M. Go, H. A. Scheraga, *Macromolecules* **1974**, *7*, 137.
- [6] D. A. McQuarrie, *Statistical Mechanics*; Harper & Row: New York, **1976**.
- [7] A. Kitao, S. Hayward, N. Go, *Proteins* **1998**, *33*, 496.
- [8] R. W. Pickersgill, *Protein Eng.* **1988**, *2*, 247.
- [9] E. L. Mehler, T. Solmajer, *Protein Eng.* **1991**, *4*, 903.
- [10] T. Solmajer, E. L. Mehler, *Protein Eng.* **1991**, *4*, 911.
- [11] D. Bashford, D. A. Case, *Annu. Rev. Phys. Chem.* **2000**, *51*, 129.
- [12] R. A. Brown, D. A. Case, *J. Comput. Chem.* **2006**, *27*, 1662.
- [13] W. C. Still, A. Tempczyk, R. C. Hawley, T. Hendrickson, *J. Am. Chem. Soc.* **1990**, *112*, 6127.
- [14] G. D. Hawkins, C. J. Cramer, D. G. Truhlar, *J. Phys. Chem.* **1996**, *100*, 19824.
- [15] H. Gohlke, C. Kiel, D. A. Case, *J. Mol. Biol.* **2003**, *330*, 891.
- [16] V. Zoete, O. Michielin, *Proteins* **2007**, *67*, 1026.
- [17] R. Geney, M. Layten, R. Gomperts, V. Hornak, C. Simmerling, *J. Chem. Theory Comput.* **2006**, *2*, 115.
- [18] H. M. Berman, J. Westbrook, Z. Feng, G. Gilliland, T. N. Bhat, H. Weissig, I. N. Shindyalov, P. E. Bourne, *Nucleic Acids Res.* **2000**, *28*, 235.
- [19] A. W. Schuttelkopf, D. M. van Aalten, *Acta Crystallogr. D Biol. Crystallogr.* **2004**, *60*(Pt 8), 1355.
- [20] J. M. Word, S. C. Lovell, J. S. Richardson, D. C. Richardson, *J. Mol. Biol.* **1999**, *285*, 1735.
- [21] D. A. Case, T. E. Cheatham, 3rd, T. Darden, H. Gohlke, R. Luo, K. M. Merz, Jr., A. Onufriev, C. Simmerling, B. Wang, R. J. Woods, *J. Comput. Chem.* **2005**, *26*, 1668.
- [22] J. Wang, P. Cieplak, P. A. Kollman, *J. Comput. Chem.* **2000**, *21*, 1049.
- [23] V. Hornak, R. Abel, A. Okur, B. Strockbine, A. Roitberg, C. Simmerling, *Proteins* **2006**, *65*, 712.
- [24] J. Wang, R. M. Wolf, J. W. Caldwell, P. A. Kollman, D. A. Case, *J. Comput. Chem.* **2004**, *25*, 1157.
- [25] L. M. McDowell, M. A. McCarrick, D. R. Studelska, W. J. Guilford, D. Arnaiz, J. L. Dallas, D. R. Light, M. Whitlow, J. Schaefer, *J. Med. Chem.* **1999**, *42*, 3910–3918.
- [26] C. I. Bayly, P. Cieplak, W. D. Cornell, P. A. Kollman, *J. Phys. Chem.* **1993**, *97*, 10269.
- [27] W. L. Jorgensen, J. Chandrasekhar, J. D. Madura, R. W. Impey, M. L. Klein, *J. Chem. Phys.* **1983**, *79*, 926.
- [28] T. Darden, D. York, L. Pedersen, *J. Chem. Phys.* **1993**, *98*, 10089.
- [29] J. P. Ryckaert, G. Ciccotti, H. J. C. Berendsen, *J. Comput. Phys.* **1977**, *23*, 327.
- [30] H. J. C. Berendsen, J. P. M. Postma, W. F. van Gunsteren, A. DiNola, J. R. Haak, *J. Chem. Phys.* **1984**, *81*, 3684.
- [31] C. S. Page, P. A. Bates, *J. Comput. Chem.* **2006**, *27*, 1990.
- [32] J. Kongsted, U. Ryde, *J. Comput. Aided Mol. Des.* **2009**, *23*, 63.
- [33] S. Fischer, J. C. Smith, S. C. Verma, *J. Phys. Chem. B* **2001**, *105*, 8050.
- [34] R. Zhou, B. J. Berne, *Proc. Natl. Acad. Sci. USA* **2002**, *99*, 12777.
- [35] R. Zhou, *Proteins* **2003**, *53*, 148.
- [36] C. Simmerling, B. Strockbine, A. E. Roitberg, *J. Am. Chem. Soc.* **2002**, *124*, 11258.
- [37] W. D. Cornell, C. I. Cieplak, I. R. Bayly, I. R. Gould, K. M. Merz, D. M. Ferguson, D. C. Spellmeyer, T. Fox, J. W. Caldwell, P. A. Kollman, *J. Am. Chem. Soc.* **1995**, *117*, 5179.
- [38] D. A. Case, *Curr Opin Struct Biol* **1994**, *4*, 285.
- [39] J. W. Pitera, W. Swope, *Proc. Natl. Acad. Sci. USA* **2003**, *100*, 7587.
- [40] A. K. Felts, Y. Harano, E. Gallicchio, R. M. Levy, *Proteins* **2004**, *56*, 310.
- [41] H. Gouda, I. D. Kuntz, D. A. Case, P. A. Kollman, *Biopolymers* **2002**, *68*, 16.
- [42] B. K. Shoichet, A. P. Graves, D. M. Shivakumar, S. E. Boyce, M. P. Jacobson, D. A. Case, *J. Mol. Biol.* **2008**, *377*, 914.
- [43] B. Kuhn, P. Gerber, T. Schulz-Gasch, M. Stahl, *J. Med. Chem.* **2005**, *48*, 4040.

Received: 2 October 2011  
Revised: 12 December 2011  
Accepted: 20 December 2011  
Published online